

Ubiquitous Spin Freezing in the Superconducting State of UTe₂

Shyam Sundar^{1,3}, Nasrin Azari¹, Mariah Goeks¹, Shayan Gheidi¹, Mae Abedi¹, Michael Yakovlev¹, Sarah R. Dunsiger^{1,2}, John M. Wilkinson⁴, Stephen J. Blundell⁴, Tristin E. Metz⁵, Ian M. Hayes⁵, Shanta R. Saha⁵, Sangyun Lee⁶, Andrew J. Woods⁶, Roman Movshovich⁶, Sean M. Thomas⁶, Priscila F. S. Rosa⁶, Nicholas P. Butch^{5,7}, Johnpierre Paglione^{5,8}, Jeff E. Sonier^{1,*}

¹*Department of Physics, Simon Fraser University, Burnaby, British Columbia V5A 1S6, Canada*

²*Centre for Molecular and Materials Science, TRIUMF, Vancouver, British Columbia V6T 2A3, Canada*

³*Instituto de Fisica, Universidade Federal do Rio de Janeiro, 21941-972 Rio de Janeiro, RJ, Brazil*

⁴*Clarendon Laboratory, University of Oxford, Department of Physics, Oxford OX1 3PU, United Kingdom*

⁵*Maryland Quantum Materials Center, Department of Physics, University of Maryland, College Park, Maryland 20742, USA*

⁶*Los Alamos National Laboratory, Los Alamos, New Mexico 87545, USA*

⁷*NIST Center for Neutron Research, National Institute of Standards and Technology, Gaithersburg, Maryland 20899, USA*

⁸*Canadian Institute for Advanced Research, Toronto, Ontario M5G 1Z8, Canada*

In most superconductors electrons form Cooper pairs in a spin-singlet state mediated by either a quantum of energy from a crystal lattice vibration (phonon) or by long-range interactions such as spin fluctuations. The novel superconductor UTe₂ is a rare material wherein electrons form pairs in a unique spin-triplet state with potential topological properties. Theoretically, spin-triplet superconductivity in UTe₂ may be explained in terms of pairing mediated by either ferromagnetic or antiferromagnetic fluctuations. Experimentally, the magnetic properties of UTe₂ remain enigmatic. Here we report muon spin rotation/relaxation (μ SR) measurements on independently grown UTe₂ single crystals that exhibit either a single or double phase transition in the specific heat near the onset of superconductivity. In the absence of an applied magnetic field, we observe an inhomogeneous distribution of magnetic fields in a sizeable volume fraction of all samples studied. The growth in the volume of the magnetic regions is halted by the onset of superconductivity at the critical temperature T_c . Upon further cooling, slow fluctuations of the local fields persist until a disordered spin frozen state appears below about one tenth of T_c . The μ SR results are consistent with the formation of magnetic clusters in UTe₂ due to the influence of disorder on long-range electronic correlations or geometrical magnetic frustration associated with the ladder-like U sublattice structure. Our findings suggest that inhomogeneous magnetic clusters are responsible for the ubiquitous residual linear term and low-temperature upturn in the temperature dependence of the specific heat in UTe₂ below T_c . The omnipresent magnetic inhomogeneity has implications for the interpretation of other low-temperature experimental observations in the superconducting state of UTe₂.

Compelling evidence for spin-triplet Cooper pairing in UTe₂ includes a large anisotropic upper critical field that greatly exceeds the Pauli paramagnetic limiting field^{1,2}, a negligible (small) change in the ¹²⁵Te-nuclear magnetic resonance (NMR) Knight shift below T_c for a magnetic field applied along the a (b or c) axis^{3,4}, and the occurrence of re-entrant superconductivity when magnetic fields as high as 60 T are applied in specific crystallographic directions^{5,6}. Moreover, the observation of chiral ingap surface states by scanning tunnelling spectroscopy suggests that UTe₂ is a spin-triplet superconductor with a nontrivial band topology⁷. Based on observations of a double phase transition in the specific heat at ambient pressure and a finite polar Kerr effect below T_c , UTe₂ is proposed to have a two-component superconducting order parameter that breaks time reversal symmetry⁸. Weyl nodes can occur in the superconducting gap for the possible two-component order parameters inferred by these data, bolstering the case for topological superconductivity in UTe₂.

Despite these developments many questions remain, including a critical one related to the underlying pairing mechanism responsible for superconductivity. Initially UTe₂ was believed to be the end member of the series of ferromagnetic (FM) uranium-based superconductors UGe₂, URhGe and UCoGe, whose spin-triplet Cooper pairing is mediated by FM fluctuations¹. Unlike the other members in this group wherein the Cooper pair spins align with the internal field generated by pre-existing FM order⁹, UTe₂ does not exhibit long-range FM order. One scenario is that superconductivity in UTe₂ is driven by strong magnetic fluctuations near a FM quantum critical point. This picture is supported by scaling of magnetization data¹ and scaling of the bulk magnetic susceptibility with the dynamic spin susceptibility¹⁰ above T_c for a field applied along the easy axis of magnetization (the crystallographic a -axis) that agree with predictions for a three-dimensional (3-D) itinerant-electron system close to a FM instability. Analogous scaling of zero-field μ SR data¹¹ down to ~ 0.4 K is also suggestive of low-frequency FM spin fluctuations that persist and coexist with superconductivity, and magnetic-field-trained polar Kerr effect measurements detect the presence of a FM susceptibility¹². In contrast, inelastic neutron scattering (INS) experiments on UTe₂ were first interpreted as a sign of dominant low-dimensional antiferromagnetic (AFM) spin fluctuations, along with an absence of FM fluctuations^{13,14}. Subsequent work has shown that the energy, momentum, and temperature dependence of these low-energy AFM-like magnetic excitations actually arises from the heavy electron band structure, and that it is not possible based on these excitations alone to conclude whether FM or AFM interactions are dominant¹⁵. In the superconducting state, a magnetic excitation near 1 meV, at finite momentum transfer, is accompanied by the apparent opening of a spin gap, which can be interpreted either as an exotic superconducting resonance or a response of the underlying magnetic fluctuations to the emergence of superconductivity^{15,16,17}. Theoretically, FM fluctuations along the a -axis are predicted at ambient pressure for itinerant f electrons in UTe₂ (ref. 18). By contrast for localized f electrons the two-leg ladder-type arrangement of the U atoms may suppress long-range magnetic order by geometrical frustration and coexisting FM and AFM fluctuations at ambient pressure and zero field are possible¹⁹. Alternatively, in this structure spin-triplet pairing may arise from the interplay between Hund's and Kondo interactions independent of the inter-site exchange (FM or AFM)²⁰. Currently there is debate on whether the double phase transition in the specific heat at ambient pressure is really a manifestation of a two-component superconducting order parameter, as two thermodynamic transitions are not observed in all UTe₂ samples and

single crystals with an optimal value of T_c near 2 K exhibit only a single-phase transition^{21,22}. The latter observation has led to the suggestion that the double transition at ambient pressure is due to an inhomogeneous distribution of two spatially separated regions of the sample with different T_c values²³. To complicate matters further, two well-defined transitions are induced by pressures above 0.3 GPa in single transition samples, with one phase transition increasing and the other decreasing with increasing pressure^{24,25}. Even UTe₂ samples that display a single-phase transition are found to exhibit an anomalous extrapolated T -linear component in the specific heat $C(T)$ below T_c , as well as a ubiquitous upturn in the specific heat at low temperatures. The coefficient of the residual T -linear term (γ^*) varies among samples but is always a substantial fraction of the normal-state value (γ_N). Both the value of T_c and the jump in the specific heat at the superconducting transition have been shown to increase with decreasing γ^*/γ_N (refs. 26, 27). While the low-temperature upturn of $C(T)$ was suggested to arise from the high-temperature tail of a nuclear Schottky anomaly, the form of the upturn varies somewhat among samples. The origins of the upturn and γ^* in UTe₂ are unsettled issues.

Other heavy-fermion superconductors, including UPt₃, URu₂Si₂, UPd₂Al₃, and CeCoIn₅ (refs. 28-31) also exhibit a large residual T -linear term in the low-temperature specific heat. Although some have proposed this to be an intrinsic property, γ^* in these other materials is also sample dependent. One potential explanation for γ^* is that there is a residual electronic contribution to $C(T)$ coming from some fraction of the sample that remains in the normal state. A residual T -linear term in the temperature dependence of the thermal conductivity $\kappa(T)$ would then be expected due to heat conduction by the unpaired ‘normal’ delocalized electrons. Another possibility is that γ^* results from resonant impurity scattering in a superconducting state with a highly anisotropic order parameter³². A finite T -linear term in $\kappa(T)$ as $T \rightarrow 0$ is likewise expected, due to broadening of the gap nodes by impurity scattering resulting in a finite residual density of states at zero energy. Yet in contrast to other heavy-fermion superconductors, a vanishingly small residual T -linear contribution to the thermal conductivity of UTe₂ is observed³³. This raises the possibility that the extrapolated T -linear component in $C(T)$ is of magnetic origin.

Here the magnetic properties of UTe₂ are addressed via a comprehensive μ SR study of independently grown single crystals that exhibit a single or double phase transition in the specific heat. The investigation of multiple samples from independent sources enables us to distinguish common trends. We show that there is a fast-relaxing component of the μ SR signal due to the development of magnetic clusters and a slower relaxing component apparently due to spins that mediate interactions between the clusters. An additional large non-relaxing component in the μ SR signal suggests that fast spin fluctuations persist down to at least ~ 0.02 K in a significant volume fraction of the sample. We find that percolation or growth of the magnetic clusters cease, and the spin dynamics of the clusters slow down with the onset of superconductivity. Eventually the magnetic clusters freeze in a gradual process at lower temperatures where the upturn in $C(T)$ occurs. We discuss how the magnetic clusters can account for the upturn and residual T -linear term in the specific heat of UTe₂.

Experimental Data

Specific heat — Figure 1a-c shows the temperature dependence of the specific heat for the samples studied here by μ SR plotted as C/T versus T . The specific heat data for sample S1 grown at UMD exhibits a double bulk phase transition and an upturn below ~ 0.3 K, whereas a single bulk phase transition is shown for samples S2 and S3 grown at LANL. Figure 1d shows C/T versus T data extending to lower temperatures for additional samples grown at UMD and LANL, and from ref. 34. Even sample S5, which exhibits a specific heat jump near 2 K shows a low-temperature upturn.

Muon spin relaxation — The photos in Fig. 1 show the samples investigated by μ SR mounted on the silver (Ag) sample holders used for measurements utilizing a dilution refrigerator. Sample S1 is a randomly oriented mosaic of 22 irregularly shaped single crystals from the same growth batch. Samples S2 and S3 are flat, plate-like single crystals that were aligned with the c -axis perpendicular to the flat surfaces. Sample S3 is a lone single crystal, whereas S2 consists of a large single crystal from a different growth batch and two small single crystals from the same growth batch as S3.

Zero field muon spin relaxation — Figures 2a and 2b shows zero-field (ZF) μ SR spectra for samples S1 and S2 as a function of temperature, respectively. In contrast to the measurements on unaligned sample S1, the ZF spectra for samples S2 and S3 were recorded with the initial muon spin polarization $\mathbf{P}(0)$ parallel to the c axis. The ZF signals for all three samples are well described by

$$a_0 P_z(t) = a_1 \exp(-\lambda_1 t) + a_2 \exp(-\lambda_2 t) + a_3, \quad (1)$$

where $P_z(t)$ is the time evolution of the muon spin polarization along the z axis, defined as the initial direction of $\mathbf{P}(0)$. The first two terms are temperature dependent and describe relaxation of the ZF signal by electronic moments in the sample. An exponential relaxation function $a_3 \exp(-\lambda_3 t)$ was used in place of the third term in the initial analysis of the ZF spectra. However, the fits for all three samples yielded a temperature-independent value of $\lambda_3 = 0.000 \pm 0.001 \mu\text{s}^{-1}$. A non-relaxing temperature independent ZF signal is expected from muons stopping in the Ag sample holder. However, for the experimental configuration utilized the amplitude of this component is much too large to be solely due to the fraction of the muons stopping outside the sample. This is evident from the photographs in Fig. 1. The non-relaxing signals from muons stopping outside and inside the sample cannot be distinguished in ZF, but their relative amplitudes are estimated using transverse-field (TF) measurements at $H = 20$ kOe to account for approximately 34 %, 30 % and 40 % of the total amplitude of the ZF signals in samples S1, S2 and S3, respectively (Extended Data). The amplitudes and relaxation rates in the first two terms of equation (1) were found to play off each other in fits with all parameters free to vary with temperature. Consequently, a_1 and a_2 were considered as temperature-independent fit parameters for sample S1, while a_1 was free to vary for samples S2 and S3, for reasons explained below. These constraints in the data analysis are considered in the interpretation of the results.

The fits to equation (1) indicate a non-relaxing signal coming from a significant volume fraction of the sample, given by the ratio $(a_3 - a_B)/a_0$ (Table 1), where a_B is the amplitude of the signal from muons stopping outside the sample. The typical relaxation of the ZF signal by randomly oriented nuclear moments is expected to be extremely weak in UTe₂. This is because the only stable uranium isotope with nonzero nuclear spin, depleted ²³⁵U, has a natural abundance of 0.20 % and the natural abundance of the tellurium isotopes with nuclear spin ¹²³Te and ¹²⁵Te are only 0.89 % and 7 %, respectively. Even so, a large temperature-independent non-relaxing signal from the sample is unexpected. It implies there are regions of the sample where either the root mean square of the local field at the muon site is extremely small or the local field fluctuates so fast that there is complete decoupling of the muon spin from the local field. In other words, even at the lowest temperature considered there are no electronic moments that are static or fluctuating slowly enough to cause a detectable relaxation of the ZF signal in a substantial portion of the sample volume.

We now consider the exponentially relaxing signals for all three samples. For the unoriented mosaic S1, approximately 27 % of the sample is described by a fast exponential relaxation rate (λ_1) and the remaining 37 % by a slower exponential relaxation rate (λ_2). Figure 2c shows the temperature dependence of λ_1 and λ_2 in sample S1, which exhibit behaviors resembling that observed in our earlier study of a different sample¹¹. The temperature dependence of λ_1/T overlaps with the earlier data above 0.75 K (Fig. 2c inset) where a fit of the current data to the relation $\lambda_1/T \propto T^{-n}$ yields $n = 1.43 \pm 0.06$ (Extended Data). While this is larger than the self-consistent renormalization (SCR) theory prediction for a 3-D metal near a FM instability³⁵ ($n = 1.33$), the value for S1 overlaps $n = 1.35 \pm 0.04$ determined in the earlier study. We note that the fast relaxation component is a smaller fraction of the total ZF signal compared to our previous study (18 % rather than 24 %) and consequently there is more scatter in the present data for $\lambda_1(T)$. Here it is now evident though that the change in the variation of λ_1/T with T at lower temperatures culminates with a saturation of λ_2 below ~ 0.2 K and a ZF signal with a single exponential relaxation component.

By contrast, there is a significant loss of the initial amplitude of the ZF signal for the *c*-axis aligned single crystals (samples S2 and S3) over the entire temperature range, with some remnant of a fast-relaxing component at early times that diminishes with decreasing temperature. The gradual loss of the fast-relaxing component in the initial dead time of the μ SR spectrometer leads to a reduction of the amplitude a_1 and a large uncertainty in the fitted value of λ_1 (Fig. 2d). The more rapid relaxation rate in the *c*-axis aligned samples implies a wider distribution of local field sensed by the muon. This may result from a slower fluctuation rate and/or an anisotropic distribution of the local fields.

The temperature dependence of λ_2 in samples S2 and S3 are quite similar. As in sample S1, λ_2 increases with decreasing temperature below 0.5 K and plateaus below ~ 0.12 K (Fig. 2d). There is also an abrupt change in the temperature dependence of λ_2 at T_c , with an initial saturation of λ_2 below T_c . The peak in λ_2 near T_c for sample S3 indicates a significant change in the dynamics of the local magnetic fields. This peak is likely smeared out in sample S2, which consists of single crystals from two different growth batches exhibiting slightly different magnitudes and widths of the specific heat jump at T_c (Fig. 1) and is entirely absent in sample S1.

Longitudinal field muon spin relaxation — Figure 3a-c shows the time evolution of the muon spin polarization in sample S1 recorded in a longitudinal-field (LF) experimental configuration with a magnetic field applied parallel to $\mathbf{P}(0)$ in three temperature regimes. At 9.5 K, an applied field of 1 kOe does not completely quench the relaxation of the LF signal, indicating the existence of rapidly fluctuating internal magnetic fields. At 0.3 K, the LF signal displays a fast-relaxing front-end and a slow decaying “tail”. The evolution of the LF signal with increasing field suggests a broad distribution of slowly fluctuating internal fields. At 0.06 K the tail of the LF signal is non-relaxing at 150 Oe, while the fast-relaxing signal persists. This indicates a broad distribution of nearly frozen internal fields. The width of the local field distribution is estimated to be ~ 260 G. The single-exponential form of the relaxing ZF signal at 0.06 K is a characteristic of dilute static magnetic moments approximated by a Lorentzian field distribution.

Figure 3d shows the field dependence of the LF signal for sample S2 well above T_c . The applied LF increasingly brings signal amplitude back from the initial dead time as the LF approaches the characteristic width of the internal magnetic field distribution. At this temperature a LF of 10 kOe is insufficient to completely suppress the muon spin depolarization, indicating there are fluctuating local fields of $\sim 10^8$ Hz in some fraction of the sample. At 0.06 K, the observable LF signal barely relaxes at 500 Oe (Fig. 3e) and hence the local fields are close to static. However, there is still some missing amplitude due to the broad distribution of local field. The LF signals in samples S1 and S2 at 0.06 K demonstrate that the saturation of the ZF relaxation rate below ~ 0.12 K is caused by a spin frozen state. As shown in Fig. 3f, a rapidly damped small-amplitude coherent precession signal is visible in the ZF signal of sample S2 at low temperatures, indicating the existence of magnetically ordered regions in the sample. The frequency of the oscillation corresponds to a local field of ~ 310 G. A similar oscillatory signal is not observed in samples S1 or S3.

Weak transverse field muon spin rotation — To gain further insight on the nature of the magnetic environment in UTe₂, measurements were performed in a weak transverse field (wTF), where the magnetic field is applied perpendicular to the initial muon spin polarization $\mathbf{P}(0)$. In a paramagnetic state the muon spin precesses around the wTF at the Larmor frequency $\omega = \gamma_\mu B_{\text{wTF}}$, where γ_μ is the muon gyromagnetic ratio and B_{wTF} is the magnitude of the wTF. In the magnetically ordered environment of UTe₂ the local magnetic field greatly exceeds the wTF and the signal is rapidly depolarized. Figure 4a shows the time evolution of the muon spin polarization in sample S2 after cooling in a wTF of 23 Oe applied in the *a-b* plane perpendicular to $\mathbf{P}(0)$. There is a clear reduction in the amplitude of the wTF signal at the lower temperature, which occurs due to muons stopping in magnetic regions of the sample where they experience a wide distribution of local fields. The wTF signals were fit to the following two-component function

$$a_{\text{wTF}} P_z(t) = a_4 \exp(-\sigma_4^2 t^2) \cos(\omega_4 t + \phi) + a_5 \exp(-\sigma_5^2 t^2) \cos(\omega_5 t + \phi). \quad (2)$$

While fits to this function provide an accurate determination of the total amplitude a_{wTF} , the signals from the paramagnetic volume fraction of the sample and muons stopping outside the sample cannot be resolved at 23 Oe. Consequently, TF measurements at 20 kOe were used to determine the ratio of the amplitude of the wTF signal from muons

stopping outside the sample (a_B) and the maximum amplitude of the wTF signal (Extended Data). Since the full amplitude of the ZF signal in samples S2 and S3 is not completely recovered at 5 K, the maximum amplitude of the wTF signal was determined in separate calibration measurements on an Ag sample (a_{Ag}) mounted on the same sample holder used for each UTe₂ sample. The magnetic volume fraction of the sample is then calculated as $V_f = (a_{Ag} - a_{wTF})/(a_{Ag} - a_B)$. For consistency, the magnetic volume fraction of the sample associated with the missing amplitude in the ZF signal is calculated assuming the same values of a_{Ag} and a_B . The calculated values of V_f show good agreement between the wTF and ZF data (Fig. 4b). Although the wTF data for sample S3 is limited, it is clear this sample has a smaller magnetic volume than sample S2. We speculate that this is the reason it has a larger specific heat jump at T_c (Fig. 1). The peak in the ZF data for V_f near T_c for sample S3 is highly correlated with the peak in λ_2 (Fig. 2d) and does not necessarily imply a peak in the magnetic volume fraction. Rather it is another indication of an abrupt change in the evolution of the magnetic regions in the sample. Similar wTF measurements were not carried out on sample S1, although the ZF data do not indicate a loss of the signal in the initial dead time, except perhaps below ~ 0.3 K where λ_1 decreases and $C(T)$ increases with decreasing temperature. We note that our previous measurements¹¹ on an unoriented single-crystal mosaic of UTe₂ with a similar value of T_c showed a reduction in the amplitude of the wTF signal at 0.25 K compared to the signal at 2.5 K.

Discussion

Density functional theory (DFT) calculations suggest a single crystallographic muon site at (0.44, 0, 0.5) in UTe₂ (Fig. 5a, b). The DFT calculations do not consider local distortions of the crystal lattice by the positive muon, which may change this site slightly. For a single muon site in the absence of long-range magnetic order, the presence of relaxing and non-relaxing components in the ZF signal from the sample means that the magnetic properties of UTe₂ are spatially inhomogeneous. The non-relaxing component suggests there are regions of the sample where the U moments fluctuate so rapidly that they are completely decoupled from the muon spin, even at millikelvin temperatures. Alternatively, if there are quasistatic magnetic moments in these regions of the sample, the magnetic moments must be very small. From the uncertainty in the fitted value of the relaxation rate of the non-relaxing signal (0.001 μs^{-1}), we estimate the width of the distribution of any quasistatic local fields of nuclear or electronic origin in the non-relaxing regions of the sample to be less than 1 mT.

Previously, we attributed the presence of two exponential relaxing components in UTe₂ to two distinct crystallographic muon sites¹¹. Since the DFT calculations suggest a single muon site and it is evident that the ratio of the two relaxation rates (λ_1/λ_2) is not independent of temperature, we consider other possibilities. In the temperature range (0.3–2 K) where two exponential relaxation rates are well resolved in sample S1, the presence of fast and slow relaxation rates is reminiscent of homogeneous spin freezing, albeit in a fraction of the sample volume. However, the amplitude of the slow-relaxing exponential “tail” of the ZF signal is greater than the amplitude of the fast-relaxing component ($a_2 > a_1$), which is not possible for random local fields and would imply a preferred orientation of the local field at the muon site with a fixed angle with respect to $\mathbf{P}(0)$ in nearly two

thirds of the sample volume. Hence, we attribute the fast-relaxing ZF signal to magnetic regions where frozen or very slow fluctuating spins generate a wide distribution of internal magnetic field and the slow-relaxing signal to paramagnetic regions of the sample where the electronic moments are fluctuating within the μ SR time window.

The fast relaxation in all three samples is presumably associated with the development of extremely slow longitudinal magnetic fluctuations along the a -axis, detected as an initial rapid growth of the ^{125}Te NMR spin-spin relaxation rate $1/T_2$ below 30-40 K for a magnetic field $H \parallel a$ axis¹⁰. Recently these slow magnetic fluctuations have been attributed to the growth of long-range FM correlations within the U-ladder sublattice structure³⁶. In this same study, a breakdown in scaling between the normal-state bulk magnetic susceptibility and ^{125}Te NMR Knight shift below ~ 10 K has been attributed to the formation of magnetic clusters by disorder/defect induced local disruptions of the long-range correlations, based on analogous behavior of low-dimensional correlated magnets with quenched disorder. Here we note that theoretically it has been shown that disorder in quasi 2-D and 3-D geometrically frustrated systems can also result in the formation of magnetic clusters of various sizes containing locally ordered spins^{37,38}. In UTe₂ the combination of potential strong magnetic frustration imposed by the staggered two-leg ladder-type arrangement of the U atoms¹⁹ (see Fig. 5c) and low-levels of disorder may induce the development of magnetic clusters.

A non-oscillating component in the wTF μ SR signal is consistent with muons stopping in or near magnetic clusters where they experience strong internal magnetic fields along the muon spin polarization and much larger than the applied field. The observation of a spontaneous spin precession signal in sample S2 below ~ 0.2 K (Fig. 3f) provides further evidence of locally ordered spins and the more rapid depolarization of the ZF signal in the c -axis aligned single crystals is presumably caused by the anisotropic internal magnetic field distribution generated by the magnetic clusters. The non-relaxing component in the ZF signal indicates that correlations of electronic moments are either absent or undisturbed in a significant volume of all three samples. In the non-relaxing regions of the sample, FM or AFM fluctuations may be present that are simply too fast to be detectable in the μ SR time window.

In contrast to NMR $1/T_2$ studies, our μ SR measurements of the magnetic properties of UTe₂ extend well below T_c . The comprehensive wTF data for sample S2 (Fig. 4b) indicates a growth in the volume of magnetic clusters with decreasing temperature, which is halted by the onset of superconductivity. The temperature dependence of λ_2 in samples S2 and S3 (Fig. 2d) appears correlated with the saturation of the magnetic volume fraction at T_c . While this behavior is more subtle in sample S1, there is some initial saturation of λ_1 below T_c (Fig. 2c) that suggests the fast and slow relaxing signals are not completely resolved near T_c where λ_2 is quite small. Above ~ 0.5 K the temperature dependence of λ_2 in samples S2 and S3 closely resembles that of the relaxation rate of the wTF signal from muons stopping in paramagnetic regions of the FM cluster-phase of $(\text{Fe}_{1-x}\text{Ni}_x)_3\text{GeTe}_2$ (ref. 39). In the latter compound the relaxation rate of the paramagnetic regions increases as the temperature is lowered, peaks at a magnetic transition temperature where the growth in the volume of magnetic clusters ceases and saturates below the transition. Hence, we attribute λ_2 in UTe₂ to the width of the motionally-narrowed field distribution of independent spins outside the magnetic clusters that

mediate interactions between them. The quantity V_f is a measure of the volume fraction of the sample occupied by the magnetic clusters. The data presented in Fig. 4b shows that V_f is smaller in sample S3, which exhibits the sharpest superconducting transition in the specific heat. However, we do not see evidence in the existing data that the saturation of V_f or slowing down of the fluctuation rate of the magnetic clusters is responsible for the double transition observed in the specific heat of sample S1.

While our previous experiment¹¹ was consistent with the variation $\lambda_1/T \propto T^{-4/3}$ predicted for a 3-D metal in proximity to a FM instability, which is quite different from the prediction $\lambda_1/T \propto T^{-3/4}$ near an AFM instability³⁵, the critical exponent determined in the present study is somewhat higher than 4/3. As mentioned earlier, this may be a consequence of a reduced sensitivity to λ_1 due to a smaller fast-relaxing ZF component. However, since λ_1 is apparently associated with slow longitudinal magnetic fluctuations along the *a*-axis, the predictions for a 3-D metallic system are probably not relevant. Furthermore, the dynamics of magnetic clusters near a quantum phase transition can be quite different and in an itinerant spin system differ from power-law behavior⁴⁰. Hence, we cannot tell from the current data whether the clusters are FM or AFM.

The upturn in the low-temperature specific heat of UTe₂ has been attributed to a nuclear Schottky anomaly associated with the splitting of the nuclear energy levels of ²³⁵U by the crystalline electric field gradient²⁷. However, as argued previously³³ and shown here (Extended Data), the upturn is too broad to be explained by a nuclear Schottky contribution and the 0.20 % natural abundance of ²³⁵U is likely not sufficient to explain its magnitude and temperature profile. The μ SR results indicate the low-temperature upturn in the specific heat is associated with the freezing of magnetic clusters. The local internal fields of the magnetic clusters may induce a splitting of degenerate ground state nuclear levels. Alternatively, the upturn may result from splitting of the (2*J* + 1)-fold degenerate energy levels of independent magnetic clusters having spin *J* by crystalline anisotropy effects⁴¹. A detailed study of the upturn as a function of applied magnetic field is needed to distinguish between these two scenarios.

Lastly, we consider the origin of the large residual *T*-linear term in the specific heat of UTe₂ below T_c . Initially this was considered intrinsic and due to a large residual density of states at the Fermi level, suggestive of a non-unitary spin-triplet pairing state^{1,2}. Yet there is no residual fermionic heat transport observed in thermal conductivity measurements that could be attributed to a lingering density of states of itinerant quasiparticles in the superconducting state³³. Furthermore, the value of γ^*/γ_N varies significantly between samples. The observation here of slowly fluctuating magnetic clusters that eventually freeze indicates that the residual *T*-linear term is at least in part magnetic in origin. A low-temperature *T*-linear term in $C(T)$ is a general property of spin glasses⁴². The broad internal field distribution sensed in our experiments is suggestive of clusters of locally ordered spins in UTe₂ behaving as spin-glass-like magnetic moments. When spin clusters are the basic entity, a *T*-linear term arises from intercluster interactions⁴³ and the disordered spins between clusters⁴⁴. The ratio of γ^*/γ_N and the ratio of V_f for samples S2 and S3 is roughly the same, suggesting the residual *T*-linear term is related to the magnetic volume fraction of the sample. However, accurate determination

of γ^*/γ_N is hindered by the nonuniversal form of the low-temperature upturn of $C(T)$ and the corresponding assumptions that are made in modelling $C(T)$ below T_c .

The gradual freezing of magnetic clusters in the superconducting state has potential implications for other experimental findings in UTe₂ at low temperatures. These include (i) the finite magnetization detected via a magnetic-field-trained polar Kerr effect^{8,12}, (ii) an unexplained reduction in the intensity of the 1 meV resonance observed by INS below ~ 0.4 K¹³, (iii) evidence of two-gap superconductivity from a low-temperature downturn in $1/T_1T$ measured by NMR³ and (iv) additional peaks that appear in the ¹²⁵Te NMR spectrum at low temperatures for $H \parallel b$ axis⁴⁵.

Methods

Single crystal growth

The UTe₂ single crystals were grown at the University of Maryland (samples S1 and S5) and Los Alamos National Laboratory (samples S2, S3 and S4) by a chemical vapor transport method. Solid pieces of depleted uranium (99.99 %) and tellurium (Alfa Aesar, 99.9999 %) were weighed in a 2:3 ratio with total mass of ~ 1 g. The elements were sealed under vacuum using a hydrogen torch in a quartz tube along with ~ 0.02 g of iodine (J.T. Baker Inc., 99.99 %) in the case of sample S1 and ~ 0.2 g of iodine (Alfa Aesar, 99.99 %) for samples S2 and S3. A temperature gradient was maintained in a multi-zone furnace for 28 days (sample S1) and 11 days (samples S2, S3 and S4). The elements were placed in the hot end of the gradient at T_i , whereas single crystals of UTe₂ were obtained at T_f , the cold end of the gradient. For sample S1: $T_i = 1060$ °C and $T_f = 1000$ °C, sample S2: $T_i = 800$ °C and $T_f = 720$ °C, sample S3: $T_i = 790$ °C and $T_f = 725$ °C, and sample S4: $T_i = 800$ °C and $T_f = 725$ °C. A modified method was used for the growth of sample S5 that will be reported⁴⁶.

Muon spin relaxation/rotation (μ SR)

The μ SR measurements on all three UTe₂ samples were carried out using an Oxford Instruments top-loading dilution refrigerator on the M15 beamline at TRIUMF, Vancouver, Canada. The air-sensitive single crystals were first mounted on a pure Ag backing plate using a 50/50 mixture of Apiezon N and Cryocon grease in a glove box with an Argon overpressure. The backing plate was subsequently thermally anchored to the Ag sample holder of the dilution refrigerator. A 12.5 \times 23 mm sample holder was used for the measurements on samples S1 and S2, while a smaller 5 \times 17 mm sample holder was used for the S3 single crystal. The 22 irregular -shaped single crystals of sample S1 formed an unaligned mosaic, whereas the three single crystals of S2 and the lone single crystal of S3 were mounted with the *c*-axis aligned parallel to the initial muon spin polarization $\mathbf{P}(0)$.

Density functional theory (DFT) calculations

To find the muon site in UTe₂, DFT calculations were performed with the QUANTUM ESPRESSO package⁴⁷. These calculations were performed using a 9 \times 6 \times 3 Monkhorst-Pack grid, and ultrasoft pseudopotentials were used to model the electronic wavefunctions

of the atoms. Specifically, the $5s$ and $5p$ electrons were treated as valence electrons for Te, and the $6s$, $7s$, $6p$, $6d$ and $5f$ electrons were treated as valence for U. The strong spin-orbit coupling in U was also included in the calculation, as was 0.01 Ry of Gaussian smearing. The kinetic energy cutoff used was 85 Ry, and the charge density cutoff was set to 850 Ry.

The total potential, consisting of the sum of the bare ionic, the exchange and correlation, and the Hartree potentials, is shown in Fig. 5a, b. The sign of the potential is chosen so that the positively charged muon is most likely to go to the position of the maximum of this potential, and as such these results show that the most likely muon stopping site is (0.44, 0, 0.5). Muons are known to distort their local environment, which may result in the actual muon site being slightly displaced from this⁴⁸⁻⁵⁰. Evaluating the extent of these distortions via a DFT relaxation calculation has proven difficult due to the larger number of electrons of the U atom and is an ongoing effort.

References

- 1 Ran, S. *et al.* Newly ferromagnetic spin-triplet superconductivity. *Science* **365**, 684-687 (2019).
- 2 Aoki, D. *et al.* Unconventional superconductivity in heavy fermion UTe₂. *J. Phys. Soc. Jpn.* **88**, 043702 (2019).
- 3 Nakamine, G. *et al.* Superconducting properties of heavy fermion UTe₂ revealed by ¹²⁵Te-nuclear magnetic resonance. *J. Phys. Soc. Jpn.* **88**, 113703 (2019).
- 4 Fujibayashi, H. *et al.* Superconducting order parameter in UTe₂ determined by Knight shift measurement. *J. Phys. Soc. Jpn.* **91**, 043705 (2022).
- 5 Ran, S. *et al.* Extreme magnetic field-boosted superconductivity. *Nat. Phys.* **15**, 1250–1254 (2019).
- 6 Knebel, G. *et al.* Field-reentrant superconductivity close to a metamagnetic transition in the heavy-fermion superconductor UTe₂. *J. Phys. Soc. Jpn.* **88**, 063707 (2019).
- 7 Jiao, L. *et al.* Chiral superconductivity in heavy-fermion metal UTe₂. *Nature* **579**, 523-527 (2020).
- 8 Hayes, I. M. *et al.* Multicomponent superconducting order parameter in UTe₂. *Science* **373**, 797-801 (2021).
- 9 Aoki, D., Ishida, K. & Flouquet, J. Review of U-based ferromagnetic superconductors: Comparison between UGe₂, UrhGe, and UcoGe. *J. Phys. Soc. Jpn.* **88**, 022001 (2019).
- 10 Tokunaga, Y. *et al.* ¹²⁵Te NMR study on a single crystal of heavy fermion superconductor UTe₂. *J. Phys. Soc. Jpn.* **88**, 073701 (2019).
- 11 Sundar, S. *et al.* Coexistence of ferromagnetic fluctuations and superconductivity in the actinide superconductor UTe₂. *Phys. Rev. B* **100**, 140502R (2019).
- 12 Wei, Di S. *et al.* Interplay between magnetism and superconductivity in UTe₂. *Phys. Rev. B* **105**, 024521 (2022).
- 13 Duan, C. *et al.* Incommensurate spin fluctuations in the spin-triplet superconductor candidate UTe₂. *Phys. Rev. Lett.* **125**, 237003 (2020).
- 14 Knafo, W. *et al.* Low-dimensional antiferromagnetic fluctuations in the heavy-fermion paramagnetic ladder compound UTe₂. *Phys. Rev. B* **104**, L100409 (2021).

- 15 Butch, N. P. *et al.* Symmetry of magnetic correlations in spin-triplet superconductor UTe₂. *npj Quantum Materials* **7**, 39 (2022).
- 16 Duan, C. *et al.* Resonance from antiferromagnetic spin fluctuations for superconductivity in UTe₂. *Nature* **600**, 636-640 (2021).
- 17 Raymond, S. *et al.* Feedback of superconductivity on the magnetic excitation spectrum of UTe₂. *J. Phys. Soc. Jpn.* **90**, 113706 (2021).
- 18 Ishizuka, J. & Yanase, Y. Periodic Anderson model for magnetism and superconductivity in UTe₂. *Phys. Rev. B* **103**, 094504 (2021).
- 19 Xu, Y., Sheng, Y., Yang, Y.-f. Quasi-two-dimensional fermi surfaces and unitary spin-triplet pairing in the heavy fermion superconductor UTe₂. *Phys. Rev. Lett.* **123**, 217002 (2019).
- 20 Hazra, T. & Coleman, P. Triplet pairing mechanisms from Hund's-Kondo models: applications to UTe₂ and CeRh₂As₂. *arXiv:2205.13529*.
- 21 Rosa, P. F. S. *et al.* Single thermodynamic transition at 2 K in superconducting UTe₂ single crystals at 2 K. *Commun. Mater.* **3**, 33 (2022).
- 22 Aoki, D. *et al.* First observation of de Haas-van Alphen effect and Fermi surfaces in unconventional superconductor UTe₂. *arXiv:2206.01363*.
- 23 Thomas, S. M. *et al.* Spatially inhomogeneous superconductivity UTe₂. *Phys. Rev. B* **104**, 224501 (2021).
- 24 Braithwaite, D. *et al.* Multiple superconducting phases in a nearly ferromagnetic system. *Commun. Phys.* **2**, 147 (2019).
- 25 Thomas, S. M. *et al.* Evidence for a pressure-induced antiferromagnetic quantum critical point in intermediate-valence UTe₂. *Sci. Adv.* **6**, eabc8709 (2020).
- 26 Aoki, D. *et al.* Spin-triplet superconductivity in UTe₂ and ferromagnetic superconductors. *JPS Conf. Proc.* **30**, 011065 (2020).
- 27 Cairns, L. P., Stevens, C. R., O'Neill, C. D. & Huxley, A. Composition dependence of the superconducting properties of UTe₂. *J. Phys.: Condens. Matter* **32**, 415602 (2020).
- 28 Fisher, R. A. *et al.* Specific heat of UPt₃: Evidence for unconventional superconductivity. *Phys. Rev. Lett.* **62**, 1411 (1989).
- 29 Fisher, R. A. *et al.* Specific heat of URu₂Si₂: Effect of pressure and magnetic field on the magnetic and superconducting transitions. *Physica B* **163**, 419 (1990).
- 30 Caspary, R. *et al.* Unusual ground-state properties of UPd₂Al₃: Implications for the coexistence of heavy-fermion superconductivity and local moment antiferromagnetism. *Phys. Rev. Lett.* **71**, 2146 (1993).
- 31 Movshovich, R. *et al.* Unconventional superconductivity in CeIrIn₅ and CeCoIn₅: Specific heat and thermal conductivity studies. *Phys. Rev. Lett.* **86**, 5152 (2001).
- 32 Hirschfeld, P. J., Wölfle P. & Einzel, D. Consequences of resonant impurity scattering in anisotropic superconductors: Thermal and spin relaxation properties. *Phys. Rev. B* **37**, 83-97 (1988).
- 33 Metz, T. *et al.* Point-node gap structure of the spin-triplet superconductor UTe₂. *Phys. Rev. B* **100**, 220504(R) (2019).
- 34 Rosuel, A. *et al.* Field-induced tuning of the pairing state in a superconductor. *arXiv:2205.04524*.
- 35 Ishigaki, A. & Moriya, T. Nuclear magnetic relaxation around the magnetic instabilities in metals. *J. Phys. Soc. Jpn.* **65**, 3402 (1996).
- 36 Tokunaga, Y. *et al.* Slow electronic dynamics in the paramagnetic state of UTe₂. *J. Phys. Soc. Jpn.* **91**, 023707 (2022).

37 Schmidt, M., Zimmer, F. M. & Magalhaes, S. G. Spin liquid and infinitesimal-disorder-driven cluster spin glass in the kagome lattice. *J. Phys.: Condens. Matter* **29**, 165801 (2017).

38 Andrade, E. C., Hoyos, J. A., Rachel, S. & Vojta, M. Cluster-glass phase in pyrochlore XY antiferromagnets with quenched disorder. *Phys. Rev. Lett.* **120**, 097204 (2018).

39 Drachuck, G. *et al.* Effect of nickel substitution on magnetism in the layered van der Waals ferromagnet Fe_3GeTe_2 . *Phys. Rev. B* **98**, 144434 (2018).

40 Vojta, T. Rare region effects at classical, quantum and nonequilibrium phase transitions. *J. Phys. A: Math. Gen.* **39**, R143-R205 (2006).

41 Falge Jr., R. L. & Wolcott, N. M. Cluster specific heats in copper-rich Cu-Ni alloys: The effect of iron. *J. Low Temp. Phys.* **5**, 617 (1971).

42 Mydosh, J. A. *Spin glasses: an experimental introduction*. (Taylor & Francis, Inc., 1993).

43 Soukoulis, C. M. & Levin, K. Cluster mean-field model of the spin glasses: static properties. *Phys. Rev. B* **18**, 1439-1445 (1978).

44 Deryabin, A. V., Rimlyand, V. I. & Larionov, A. P. Features of the change in the specific heat in magnetic phase transitions in alloys with a mixed exchange interaction. *Zh. Eksp. Teor. Fiz.* **84**, 2228-2234 (1983).

45 Nakamine, G. *et al.* Inhomogeneous superconducting state probed by ^{125}Te NMR on UTe_2 . *J. Phys. Soc. Jpn.* **90**, 064709 (2021).

46 unpublished.

47 Giannozzi, P. *et al.* QUANTUM ESPRESSO: a modular and open-source software project for quantum simulations of materials. *J. Phys.: Condens. Matter* **21**, 395502 (2009).

48 Möller, J. S., Ceresoli, D., Lancaster, T., Marzari, N. & Blundell, S. J. Quantum states of muons in fluorides. *Phys. Rev. B* **87**, 121108 (2013).

49 Foronda, F. R. *et al.* Anisotropic local modification of crystal field levels in Pr-based pyrochlores: A muon-induced effect modeled using density functional theory. *Phys. Rev. Lett.* **114**, 5 (2015).

50 Wilkinson, J. M., Pratt, F. L., Lancaster, T., Baker, P. J. & Blundell, S. J. Muon sites in PbF_2 and YF_2 : Decohering environments and the role of anion Frenkel defects. *Phys. Rev. B* **104**, L220409 (2021).

Acknowledgements

J.E.S. and S.R.D. acknowledge support from the Natural Sciences and Engineering Research Council of Canada. Research at the University of Maryland was supported by the Department of Energy Award No. DE-SC-0019154 (low temperature experiments), the Gordon and Betty Moore Foundation's EPiQS Initiative through Grant No. GBMF9071 (materials synthesis), NIST, and the Maryland Quantum Materials Center. S.R.S. acknowledges support from the National Institute of Standards and Technology Cooperative Agreement 70NANB17H301. S.J.B. and J.M.W. acknowledge support from EPSRC (Grant No. EP/N023803/1). The DFT+ μ calculations were performed on the Redwood Cluster at the University of Oxford. Work at Los Alamos National Laboratory (LANL) was performed under the auspices of the U.S. Department of Energy, Office of Basic Energy Sciences, Division of Materials Science and Engineering project "Quantum

Fluctuations in Narrow-Band Systems.” S.L. and A.W. acknowledge support from the Laboratory Directed Research and Development program at LANL.

Contributions

S.R.S. and P.F.S.R. grew the single crystals. S.R.S., T.E.M., I.M.H., P.F.S.R., S.M.T., S.L., A.W. and R.M. performed the specific heat measurements. J.E.S., N.A., M.G., S.G., M.A., M.Y., S.R.D. and S.S. performed the μ SR experiments. J.E.S., S.G. and S.S. analyzed the μ SR data. J.M.W. and S.J.B. performed the DFT calculations. J.E.S., S.R.D., J.M.W., S.J.B., S.R.S., J.P., N.P.B., S.M.T. and P.F.S.R. contributed to the writing of the manuscript.

Corresponding authors

Correspondence and requests for materials should be addressed to J.E.S. (jsonier@sfu.ca).

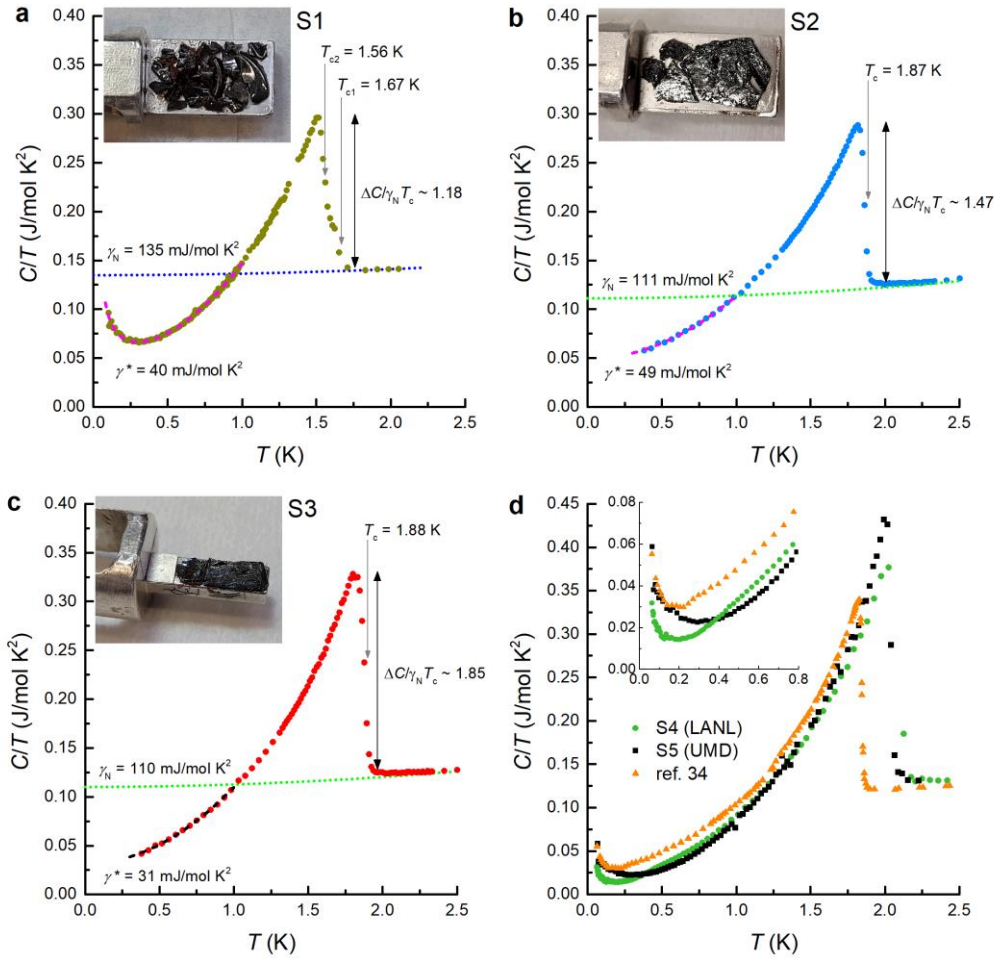


Fig. 1 | Zero-field specific heat of the UTe_2 single crystals as a function of temperature. Samples **a**, **S1** **b**, **S2**, and **c**, **S3** studied by μSR . The dotted curves are fits of the data above T_c to $C/T = \gamma_N + \alpha T^2$ and the dashed curves are fits below 1 K to $C/T = \gamma^* + \beta T^2 + A/T$. Fits of the existing data for samples **S2** and **S3** below 1 K yielded $A = 0$, compared to $A = 5.31 \text{ mJ K}^{-1}$ for sample **S1**. The photos in **a**, **b**, and **c** show the samples attached on the dilution refrigerator Ag sample holders used for the μSR measurements. The photo in **b** shows two pieces of a large **S2** single crystal that broke and two small single crystals in the upper left from the same growth batch as **S3**. The photo in **c** is a lone **S3** single crystal mounted on a smaller Ag sample holder. This crystal also broke when mounted. The fitted values of γ^* for samples **S1**, **S2** and **S3** are shown in Table 1. **d**, Additional specific heat data for independently grown samples at the University of Maryland (UMD) and Los Alamos National Laboratory (LANL), and from ref. 34.

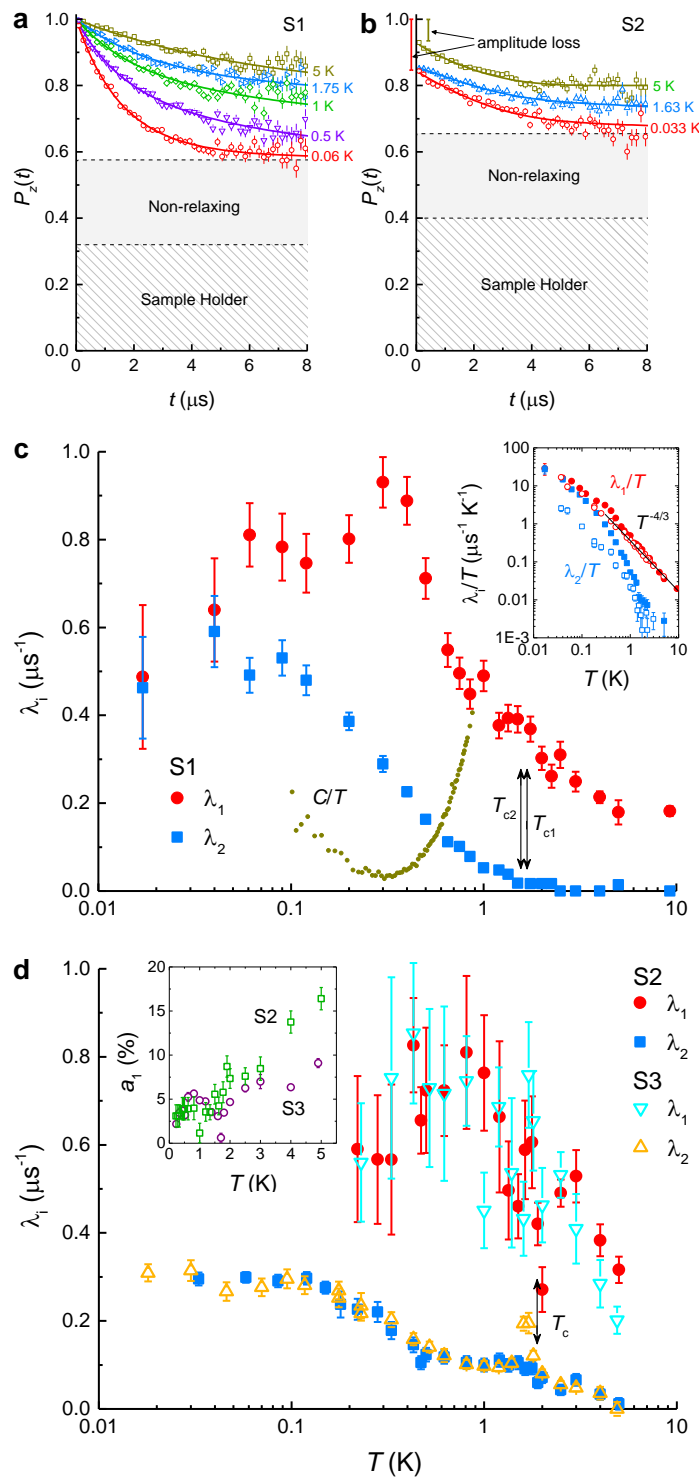


Fig. 2 | Muon spin relaxation rate of UTe_2 single crystals in zero external magnetic field. **a**, Representative ZF- μ SR spectra of samples S1 and **b**, S2 for various temperatures. The size of the non-relaxing contributions to the spectra from the sample and the sample holder are indicated by the shaded regions. For sample S2 there is a loss of initial amplitude as indicated. **c**, Temperature dependence of the ZF exponential relaxation rate λ_i (μs^{-1}) versus temperature T (K) for samples S1 and S2. The inset shows λ_i/T ($\mu\text{s}^{-1}\text{K}^{-1}$) versus T (K) with a $T^{-4/3}$ fit. **d**, Temperature dependence of the ZF exponential relaxation rate λ_i (μs^{-1}) versus temperature T (K) for samples S2, S3, and S4. The inset shows a_1 (%) versus T (K) for S2 and S3.

rates for S1 from fits of the ZF- μ SR spectra to equation (1). Also shown is the C/T versus T data for sample S1 below 0.9 K, highlighting the low-temperature upturn (For visual clarity the vertical scale of the specific heat data is not shown). The inset shows that the temperature dependence of λ_1/T and λ_2/T for sample S1 (solid symbols) compared to the sample investigated in our earlier study¹¹ (open symbols). The solid line shows the proportional relationship $\lambda_1/T \propto T^{-4/3}$ predicted by the self-consistent renormalization theory for a 3-D metal near a FM instability³⁵. **d**, Temperature dependence of the ZF exponential relaxation rates for samples S2 and S3. The inset shows the temperature dependence of the remnant amplitude a_1 of the fast-relaxing component (as a percentage of the total ZF signal amplitude). Below 0.2 K the fast-relaxing signal is completely lost in the initial dead time.

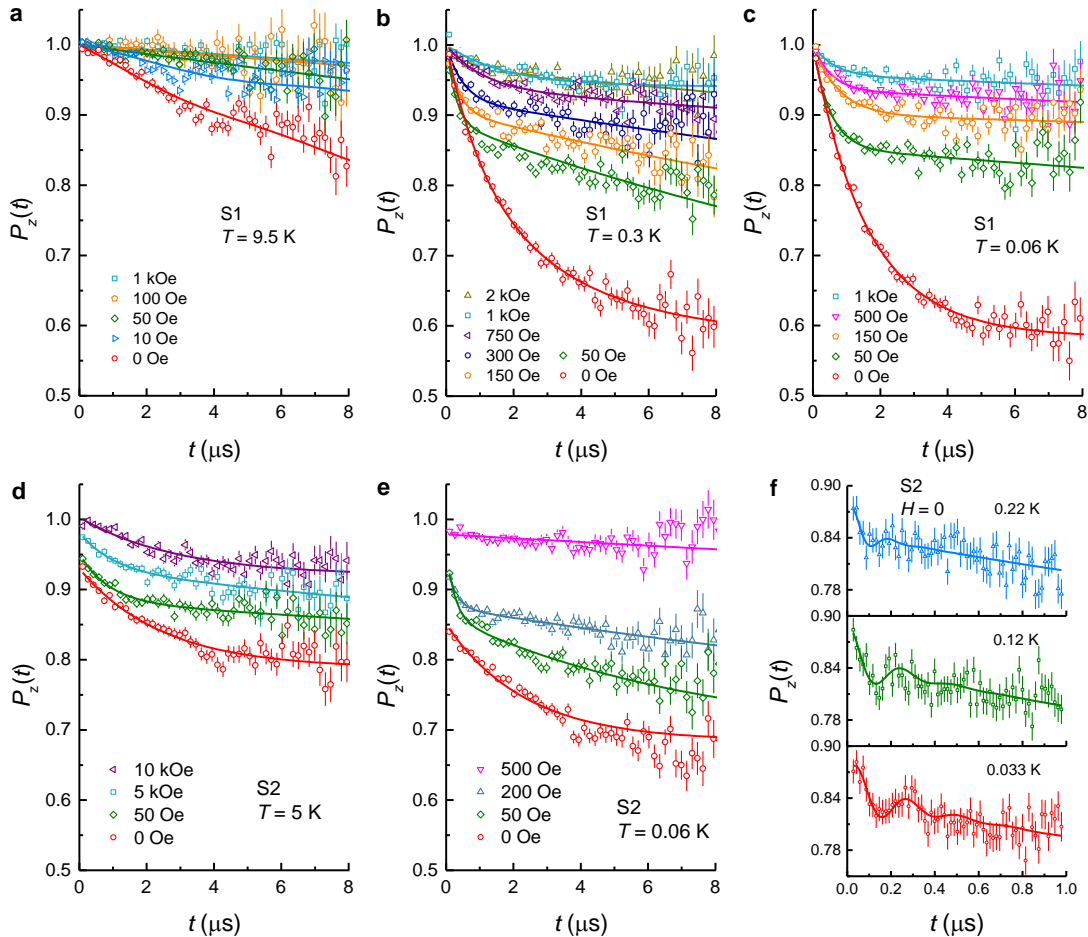


Fig. 3 | Evidence for a nearly spin-frozen state. LF- μ SR spectra recorded for sample S1 at **a**, 9.5 K, and below T_c at **b**, 0.3 K and **c**, 0.06 K for various applied magnetic fields. LF- μ SR spectra for sample S2 at **d**, 5 K and below T_c at **e**, 0.06 K for various magnetic fields applied parallel to the c -axis. **f**, ZF signals in sample S2 at early times showing an oscillatory component indicative of short-range magnetic order.

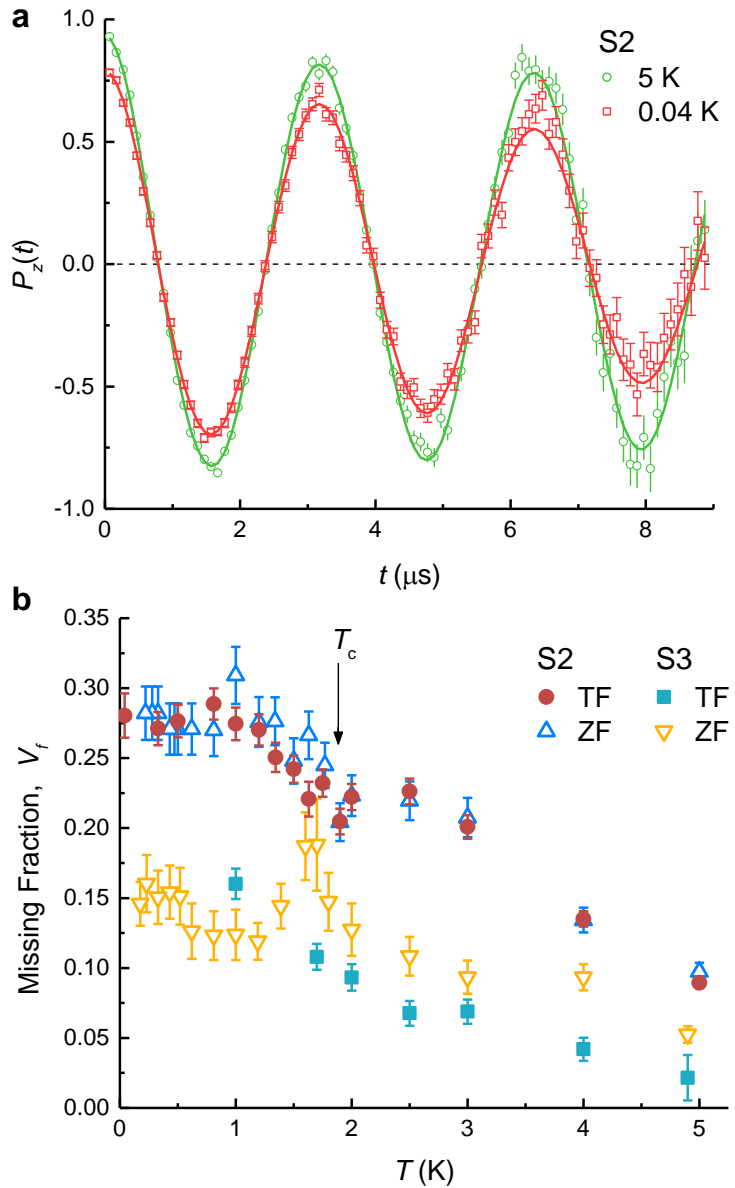


Fig. 4 | Magnetic volume fraction in c -axis aligned UTe_2 single crystals exhibiting a single-phase transition in the specific heat. **a**, Time evolution of the muon spin polarization for sample S2 recorded at 5 K and 0.04 K for a weak magnetic field $B_{\text{ext}} = 23$ Oe applied in the a - b plane perpendicular to $\mathbf{P}(0)$ and parallel to the c -axis. A portion of the signal is completely depolarized in the initial dead time of the spectrometer. **b**, Temperature dependence of the volume fraction of samples S2 and S3 responsible for the loss of asymmetry in the weak TF and ZF measurements.

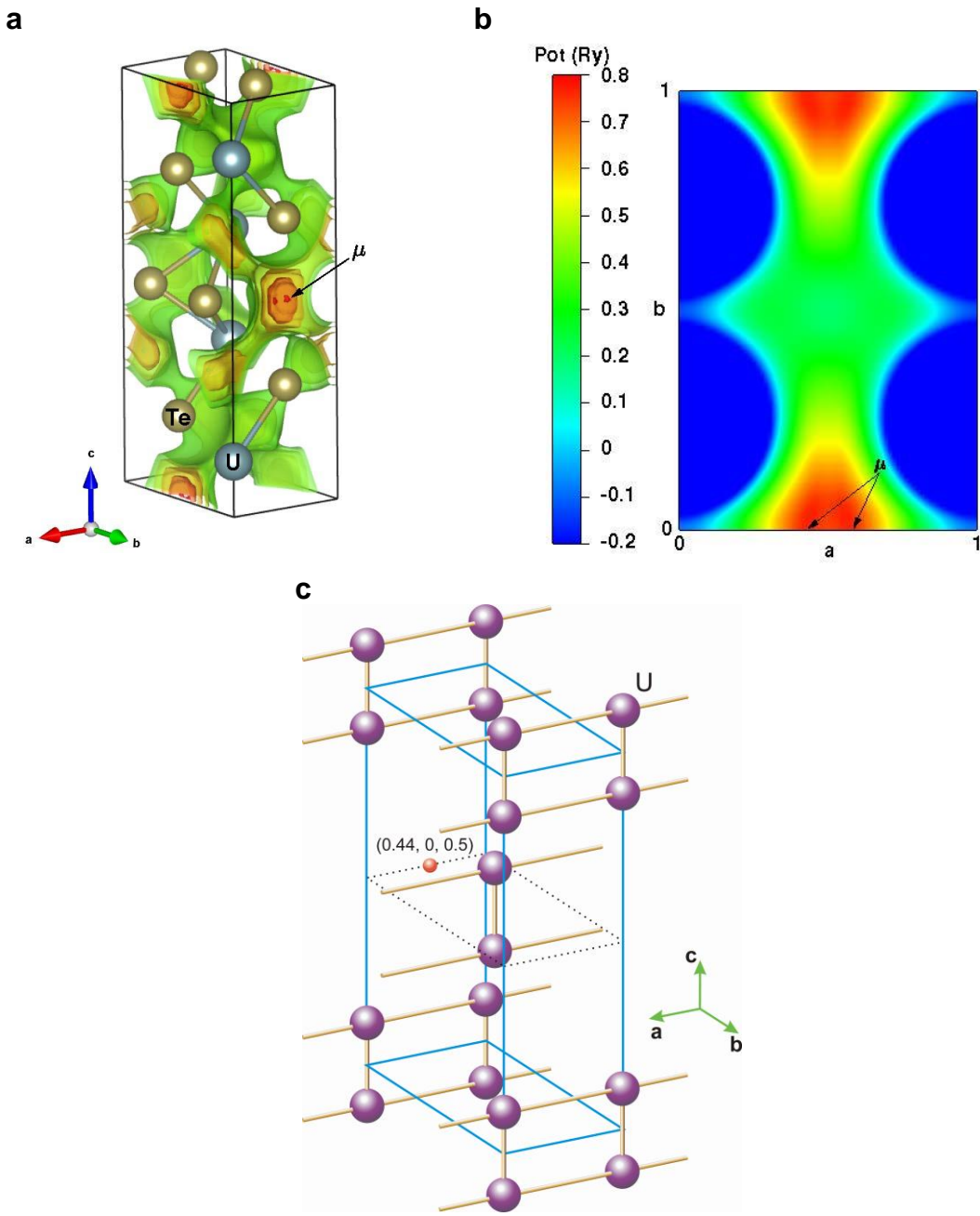


Fig. 5 | Muon site in UTe₂. **a**, Contours of the total potential calculated by DFT, and **b**, this same potential in the (0, 0, 2) plane. The energies in both figures are shaded according to the legend in the center, although energies lower than 0.4 Ry are unshaded in **a** for visual clarity. The calculated muon site at (0.44, 0, 0.5) is indicated and in **b** this is indicated along with the crystallographic equivalent site at (0.56, 0, 0.5). **c**, The staggered two-leg ladder-type arrangement of the U atoms in UTe₂. Note the ‘ladder legs’ are parallel to the *a*-axis. For visual clarity the Te atoms are not shown. The small orange sphere indicates the calculated muon site at (0.44, 0, 0.5).

Table 1 Comparison of specific heat and μ SR parameters.

	S1	S2	S3
T_c (K)	—	1.87	1.88
T_{c1}, T_{c2} (K)	1.67, 1.56	—	—
ΔT_c (K)	0.04, 0.05	0.05	0.05
γ_N (mJ/mol K ²)	135	111	110
γ^* (mJ/mol K ²)	40, 51*	49	31
γ^*/γ_N	0.30, 0.38	0.44	0.28
$\Delta C/\gamma_N T_c$	1.18	1.47	1.85
a_1/a_0	0.27	—	—
a_2/a_0	0.37	0.17	0.24
$(a_3 - a_B)/a_0$	0.36	0.52	0.46
V_f	—	0.28	0.16

The superconducting transition temperature(s) and transition width, the coefficient of the T -linear term in $C(T)$ above and below T_c , the specific heat jump at T_c , the ratio of the amplitudes of the three components in Eq. (1) to the total sample amplitude a_0 and the magnetic volume fraction at low temperatures. *From fits of $C(T)$ below 1 K assuming the full analytical expression for a two-level Schottky anomaly (Extended Data).

Extended Data

Fits of the low-temperature specific heat data for sample S1

Figure 6 shows various fits of the temperature dependence of the specific heat of sample S1 between 0.1 and 1 K. The fit assuming the full analytical expression for the Schottky anomaly of a two-level system falls well below the data point at 0.1 K.

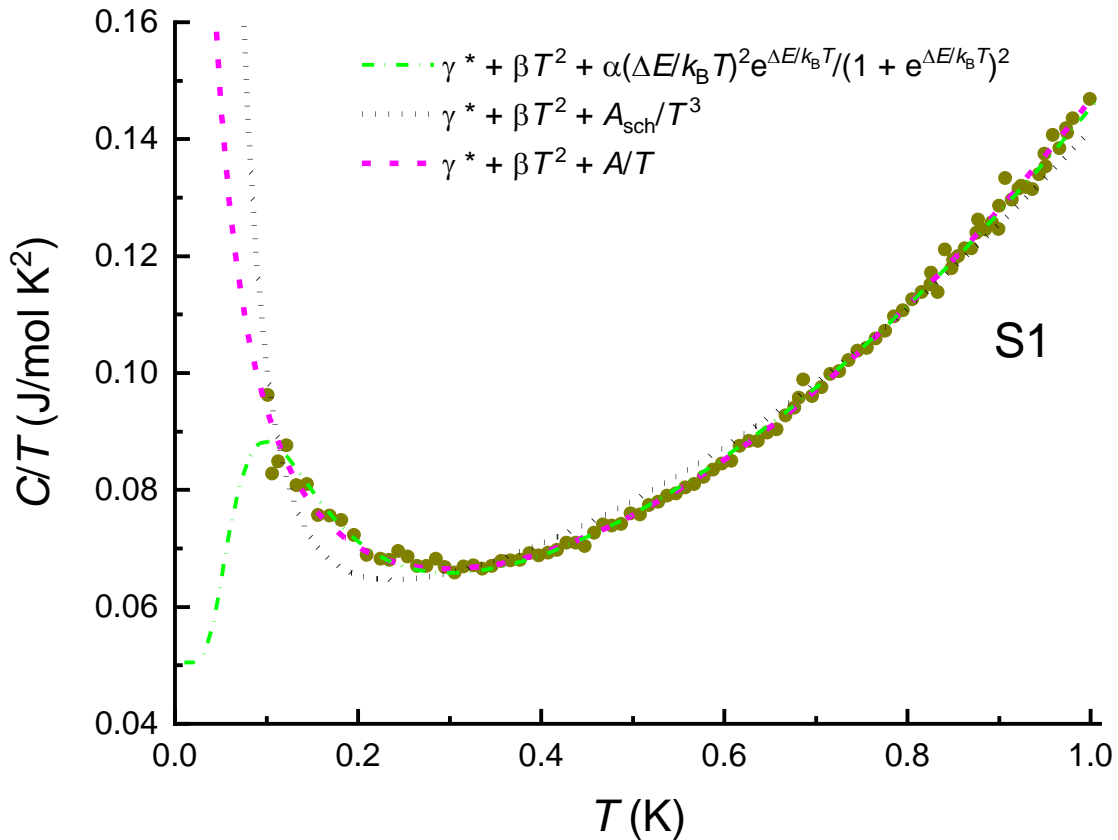


Fig. 6 | Fits of C/T versus T for sample S1 to the sum of $\gamma^* + \beta T^2$ and a third component assuming (i) the full analytical relation for the Schottky anomaly of a two-level system (dash-dotted curve), which yields $\gamma^* = 50.5$ mJ/mol K², (ii) the high-temperature tail of a Schottky anomaly for a two-level system (dotted curve), which yields $\gamma^* = 56.6$ mJ/mol K², and (iii) the term A/T (dashed curve), which yields $\gamma^* = 39.6$ mJ/mol K².

High transverse-field measurements

Transverse-field (TF) μ SR asymmetry spectra for the three UTe₂ samples in an applied magnetic field of $H = 2$ T and at a temperature above T_c are presented in Fig. 7a. The solid curves through the data points are fits to

$$A(t) = a_B \exp(-\Delta_B^2 t^2) \cos(2\pi f_B t + \phi) + \sum_{i=1}^n a_i \exp(-\Delta_i^2 t^2) \cos(2\pi f_i t + \varphi). \quad (3)$$

The first term is a background component due to muons that missed the sample and stopped in the Ag sample holder. Here a_B is the amplitude of the background signal, ϕ is the angle between the axis of the positron detector and the initial muon-spin polarization $\mathbf{P}(0)$, and f_B is the precession frequency of the muon spin in the magnetic field \mathbf{B} . The Gaussian relaxation function $\exp(-\Delta_B^2 t^2)$ is intended to account for the distribution of internal magnetic field, associated with randomly oriented nuclear moments in the sample holder, although the value of Δ_B is influenced somewhat by dipolar fields emanating from the sample associated with the field-induced polarization of the local U electronic moments. The second term, which is a sum of n similar Gaussian damped cosine functions, describes the TF- μ SR signal from muons stopping in the sample. The sample component of the signal for UTe₂ samples S1, S2 and S3 is comprised of $n = 3, 2$, and 2 components, respectively. The fitted parameters are listed in Table 2.

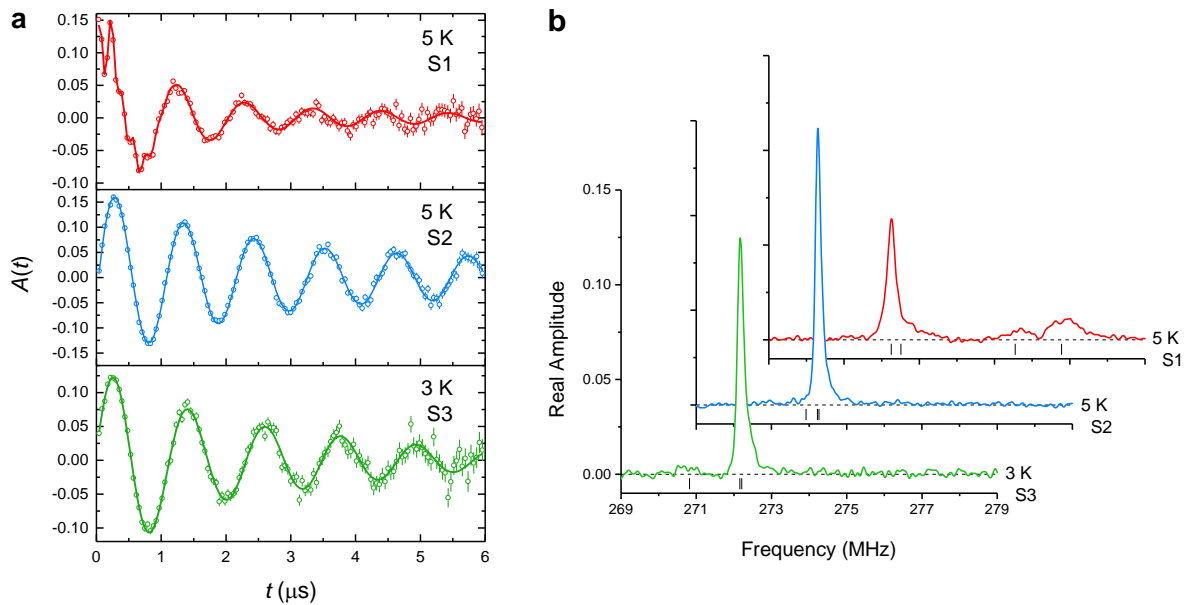


Fig. 7 | a, TF- μ SR asymmetry spectra for an applied magnetic field of $H = 2$ T recorded at temperatures above T_c . The solid curves are fits to the sum of Gaussian damped cosine functions. **b**, Fourier transforms (with Gaussian apodization) of the TF- μ SR asymmetry spectra, which provide visual depictions of the internal magnetic field distribution $n(B)$ sensed by the muon ensemble. The frequency (horizontal axis) is related to the local internal magnetic field via the relation $f = (\gamma_\mu/2\pi)B$. The vertical black lines denote the average frequencies of the multiple components that describe the TF- μ SR spectra.

Fourier transforms of the TF- μ SR signals, which provide an approximate visual representation of the internal magnetic field distribution sensed by the muon ensemble, are shown in Fig. 7b. The additional broad higher-frequency peaks for sample S3 are presumably due to the misalignment of the single crystals in the mosaic, which results in different orientations of the magnetic dipole field from the local U moments in the individual crystals.

Sample	Frequencies (MHz)	Amplitudes (%)	Relaxation Rates (μs^{-1})
S1	$f_B = 272.255(2)$	$a_B = 34(1)$	$\Delta_B = 0.44(1)$
	$f_1 = 272.51(3)$	$a_1 = 31(1)$	$\Delta_1 = 2.2(1)$
	$f_2 = 275.55(4)$	$a_2 = 13.0(1)$	$\Delta_2 = 1.8(2)$
	$f_3 = 276.78(2)$	$a_3 = 22(1)$	$\Delta_3 = 1.57(8)$
S2	$f_B = 272.221(2)$	$a_B = 30(1)$	$\Delta_B = 0.05(1)$
	$f_1 = 271.92(5)$	$a_1 = 21(1)$	$\Delta_1 = 3.6(2)$
	$f_2 = 272.261(5)$	$a_2 = 49(1)$	$\Delta_2 = 0.50(4)$
S3	$f_B = 272.1558(2)$	$a_B = 40(2)$	$\Delta_B = 0.20(1)$
	$f_1 = 270.82(6)$	$a_1 = 13(2)$	$\Delta_1 = 2.0(3)$
	$f_2 = 272.21(1)$	$a_2 = 47(2)$	$\Delta_2 = 0.80(3)$

Table 2. Parameters from fits of TF- μ SR asymmetry spectra in Fig. 7a to Eq. (3).

Fits of λ_1/T versus T for sample S1

Figure 8a shows the fit of λ_1/T versus T above 0.4 K to the relation $\lambda_1/T \propto T^{-n}$ from our previous ZF- μ SR study of UTe₂ (ref. 11). Figure 8b shows a comparison of λ_1/T versus T between the current results for sample S1 and the previous study of a different sample. There is good agreement between the two data sets above 0.75 K. The divergence of the two data sets below 0.75 K signifies a difference in the range of temperature over which the spins (magnetic clusters) freeze. Figure 8c shows a fit of λ_1/T versus T for sample S1 above 0.75 K to the relation $\lambda_1/T \propto T^{-n}$.

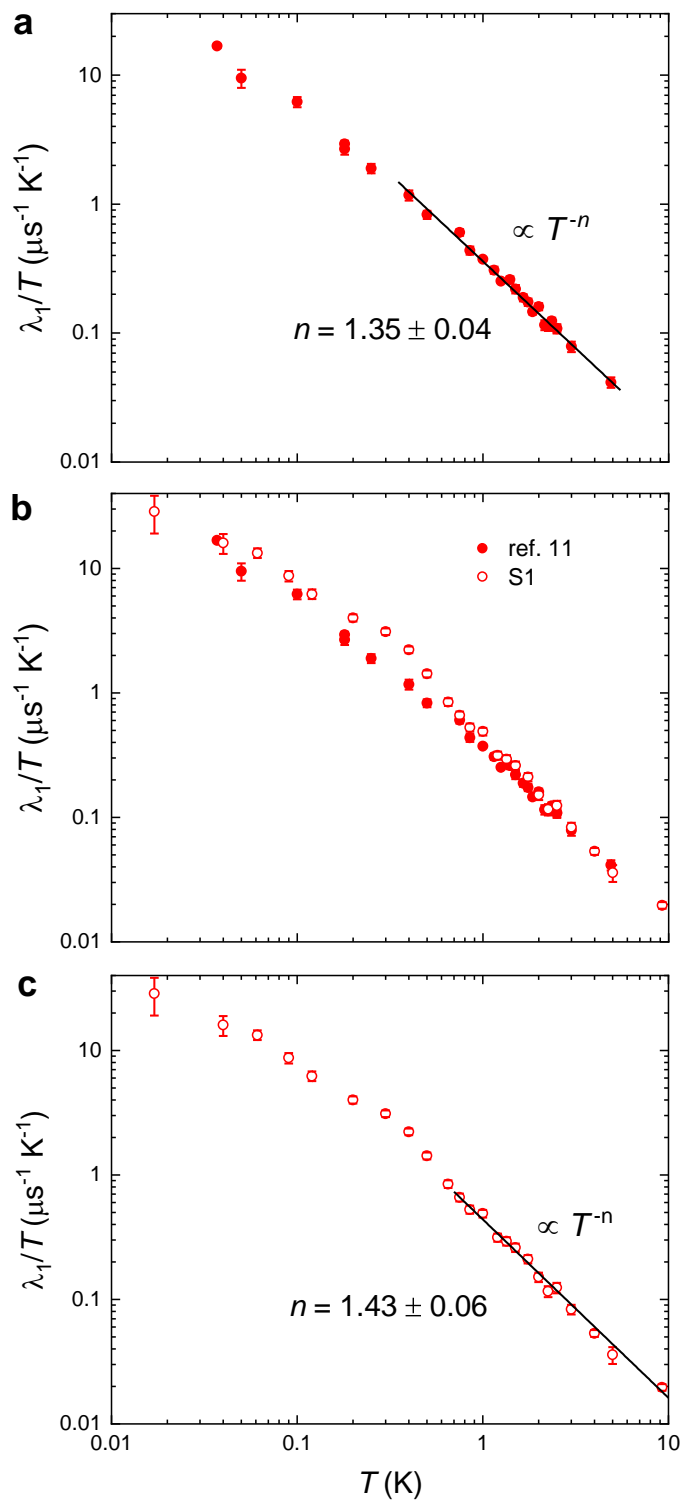


Fig. 8 | **a**, Fit of λ_1/T versus T above 0.4 K to the relation $\lambda_1/T \propto T^{-n}$ from ref. 11. **b**, Comparison of λ_1/T versus T for sample S1 to data from ref. 11. **c**, Fit of λ_1/T versus T for sample S1 above 0.75 K to the relation $\lambda_1/T \propto T^{-n}$.